NANO LETTERS

pubs.acs.org/NanoLett Letter

Fermi Pressure and Coulomb Repulsion Driven Rapid Hot Plasma Expansion in a van der Waals Heterostructure

Junho Choi, Jacob Embley, Daria D. Blach, Raül Perea-Causín, Daniel Erkensten, Dong Seob Kim, Long Yuan, Woo Young Yoon, Takashi Taniguchi, Kenji Watanabe, Keiji Ueno, Emanuel Tutuc, Samuel Brem, Ermin Malic, Xiaoqin Li,* and Libai Huang*

Cite This: *Nano Lett.* 2023, 23, 4399−4405 Read Online

ACCESS | Metrics & More | Article Recommendations | Supporting Information

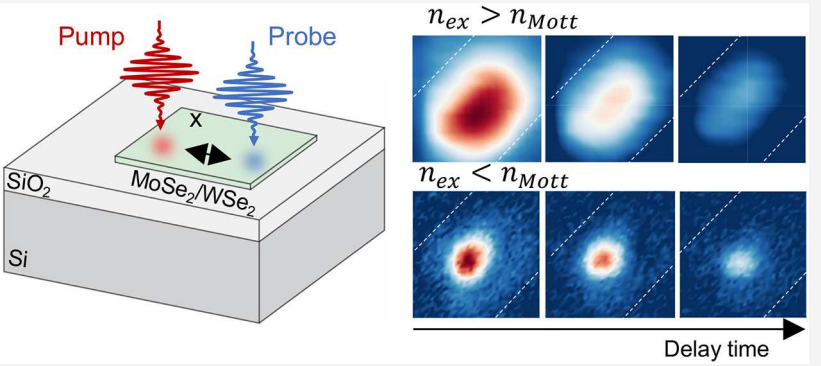

ABSTRACT: Transition metal dichalcogenide heterostructures provide a versatile platform to explore electronic and excitonic phases. As the excitation density exceeds the critical Mott density, interlayer excitons are ionized into an electron−hole plasma phase. The transport of the highly non-equilibrium plasma is relevant for high-power optoelectronic devices but has not been carefully investigated previously. Here, we employ spatially resolved pump−probe microscopy to investigate the spatial-temporal dynamics of interlayer excitons and hot-plasma phase in a $MoSe_2/WSe_2$ twisted bilayer. At the excitation density of $\sim 10^{14}$ cm^{-2}, well exceeding the Mott density, we find a surprisingly rapid initial expansion of hot plasma to a few microns away from the excitation source within ∼0.2 ps. Microscopic theory reveals that this rapid expansion is mainly driven by Fermi pressure and Coulomb repulsion, while the hot carrier effect has only a minor effect in the plasma phase.

KEYWORDS: *$MoSe_2$, WSe_2, transition metal dichalcogenides, van der Waals heterostructure, exciton*

In a type-II transition metal dichalcogenide (TMD) heterostructure, a rapid charge transfer following optical excitation leads to the formation of interlayer excitons (IXs).[1] IXs can be long-lived with their lifetimes controllable by the twist angle, making them ideal to realize quasi-equilibrium phases.[2] Indeed, a rich variety of excitonic phases (e.g., exciton insulators[3] and condensates[4−7]) have been proposed and realized in TMD heterobilayers. Depending on the exciton density, several distinct phases of localized excitons, mobile exciton gases, and ionized hot plasma have been observed in heterostructures.[8−14] At low excitation density, IXs can be localized by moiré potential in heterostructures with a small twist angle and relatively large supercells (∼10 nm).[15] As the supercell sizes reduces or exciton density increases, IXs may become a mobile exciton gas.[16] At even higher densities, the dissociation of excitons occurs at the Mott transition, where the Mott density is estimated to be between 10^{12} and 10^{13} cm^{-2} by $n_{\mathrm{Mott}}a_x^2 \sim 0.02$ with an exciton Bohr radius a_x of 1−2 nm.[17] Few optical experiments have been performed at very high excitation density beyond the Mott transition. Interestingly, new many-body ground states in TMDs, such as superconductivity, are observed at high carrier density of 10^{14} cm^{-2}, only achieved using ionic liquid gating previously.[18−21]

Here, we perform spatially resolved resonant pump−probe microscopy measurements on a near hexagonal-stacked (*H*-stacked) $MoSe_2/WSe_2$ twisted bilayer (TBL) and investigate the transport of excitons and hot plasma as a function of excitation density. At low excitation density, no obvious time evolution of the spatial distribution was observed over ∼1 ns time scale, indicating that interlayer excitons are trapped by the moiré potential, consistent with previous experiments.[9,16] At

Received: February 20, 2023
Revised: May 1, 2023
Published: May 8, 2023

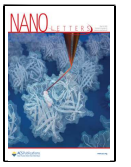

https://doi.org/10.1021/acs.nanolett.3c00678
Nano Lett. 2023, 23, 4399−4405

excitation densities well exceeding the Mott transition, we observe a remarkably fast initial expansion of hot plasma that extends several microns away from the pump laser spot within ~0.2 ps. The rapid hot plasma expansion is modeled by a microscopic theory that takes into account both electron−electron repulsion and Fermi pressure driven expansion. Fermi pressure originates from the significantly higher free energy of a quantum gas than a classical gas at the onset of degeneracy. At a sufficiently high density, Pauli's exclusion principle needs to be explicitly taken into account when describing density-dependent carrier diffusion. This carrier density can only be reached in TMD heterostructures, not in monolayers (MLs). Thus, our paper reveals unique advantages of TMD heterostructures in high power optoelectronics.

We briefly describe the sample preparation and characteristics. As illustrated in Figure 1a, the $MoSe_2/WSe_2$ TBL is

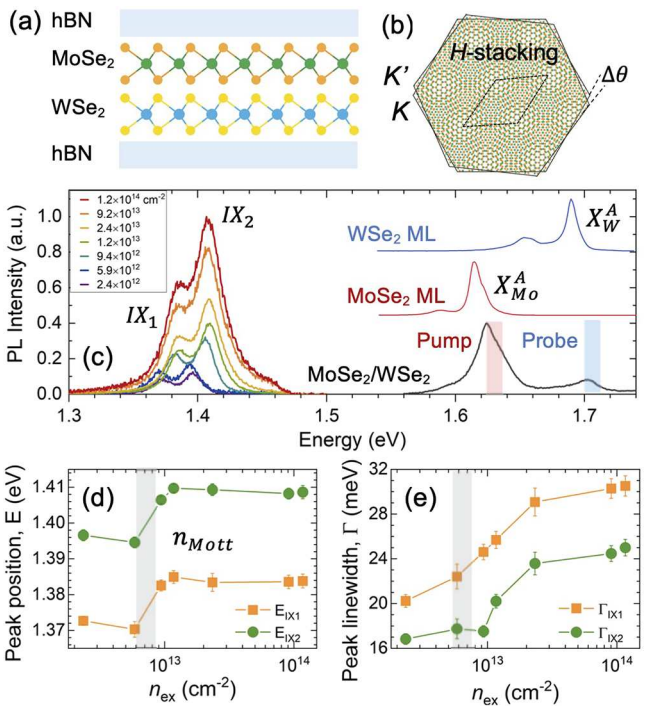

Figure 1. Identifying the Mott transition in a near-*H* stacked $MoSe_2/WSe_2$ bilayer. (a) Layered structure and (b) moiré pattern of the hBN-encapsulated $MoSe_2/WSe_2$ TBL with a near *H*-stacked configuration. The black diamond represents one supercell. (c) PL spectra taken at 78 K from ML and TBL regions. Excitation density-dependent PL spectra of the two prominent IX peaks (IX_1 and IX_2) are further analyzed in (d) peak position and (e) linewidth (full width at half-maximum, FWHM). Vertical gray shaded area indicates the excitation density at the Mott transition n_{Mott}.

encapsulated by hexagonal boron nitride (hBN) layers using a dry transfer technique (more details in Supporting Information (SI)).[22] The stacking style and twist angle were determined by second harmonic generation (SHG) to be near *H*-stacked with a twist angle of $\theta = 58.9 \pm 0.3°$ (more details in SI). At this twist angle, the calculated size of the moiré supercell is ~17 nm (Figure 1b), larger than the expected Bohr radius (~1−2 nm) of the excitons.[17]

We first perform power-dependent photoluminescence (PL) experiments (Figure 1c) to identify the relevant excitonic resonances and the Mott transition. All measurements are performed at low temperature, $T = 78$ K, unless stated otherwise. PL spectra taken from the WSe_2 and $MoSe_2$ ML regions of the sample are dominated by neutral and charged A-excitons, which we label as X^A_W and X^A_{Mo}. For spectra taken within the TBL region, the intralayer excitons are energetically similar to the A-excitons from the corresponding MLs. Two prominent IX resonances are observed in the PL (Figure 1c) and we attribute them to the singlet (IX_2) and triplet (IX_1) IX states, consistent with other spectroscopic studies of near *H*-stacked $MoSe_2/WSe_2$ TBLs.[23−25] The excitation density-dependent PL measurements are taken by tuning the laser to the A-exciton resonance of ML $MoSe_2$. We fit multiple Gaussian functions to extract the central energy and FWHM of the two IXs as shown in Figure 1d-e. A sudden change in both the resonant energy and FWHM of the IX resonances is observed at a density $\sim 7 \times 10^{12}$ cm^{-2}. While repulsive dipolar interactions, bandgap renormalization, and decreased exciton binding energy can all lead to spectral shifts in exciton resonant energy, this sudden jump in energy and spectral broadening has been considered as a signature of screening from the dissociated excitons.[13,26,27] We designate this excitation density as the onset of the Mott transition in the rest of this paper. Previous studies have identified the excitation density of $\sim 10^{13}$ cm^{-2} as the onset of the Mott transition,[28−31] which is within the range of uncertainty due to exciton Bohr radius, exciton creation under nonresonant excitation, the onset of resonance shift, and linewidth broadening in Figure 1d,e. Next, we apply a spatially resolved pump probe microscopy technique to map the transport of carriers and/or excitons. The experimental setup is described in detail in the SI. The pump/probe technique used here is also referred to as differential reflectance and detects a third-order nonlinear signal. Briefly, co-circularly polarized pulses are used as pump and probe beam for the measurements. A spatial resolution of ~200 nm and a temporal resolution of ~0.2 ps are achieved. The pump energy was tuned to 1.62 eV, resonant with A-exciton in $MoSe_2$ ML, while the probe energy was centered near 1.70 eV, resonant with the A-excitons in WSe_2 ML (Figure 1c). Because the oscillator strength associated with IXs are small due to their spatially indirect nature, IX resonances are not directly observable in resonant pump probe spectra.

Although the probe wavelength is tuned to be resonant with the intralayer exciton, the probe absorption and detected nonlinear signal are additionally sensitive to excess holes in the WSe_2 layer and IXs that form following pump excitation and subsequent charge transfer. This expanded probe sensitivity results from a phase space filling effect as illustrated in Figure 2a. The hypothesis that free carriers or IXs dominate the nonlinear signal at long delay times is supported by the measured long-lived nonlinear signal (details in SI) and the known large oscillation strength of intralayer excitons, which leads to a short radiative lifetime (<1 ps) and an even shorter total population relaxation time.[2,32] Thus, the long-lived nonlinear signal observed in our experiments can only be explained by the long-lived excitations of free holes and IXs.[9,33]

The transport of ionized holes or IXs is imaged by scanning the probe beam while keeping the pump beam fixed (Figure 2b). The images taken at three excitation densities, 3×10^{14}, 3×10^{12}, and 4×10^{11} cm^{-2}—above and below the Mott density—are presented in Figure 2c−e, respectively. The excitation densities quoted here are calculated by the average excitation powers used (details in SI). The diffusion images at different excitation densities are strikingly different. At the highest density shown in Figure 2c, the carrier distribution

https://doi.org/10.1021/acs.nanolett.3c00678
Nano Lett. 2023, 23, 4399−4405

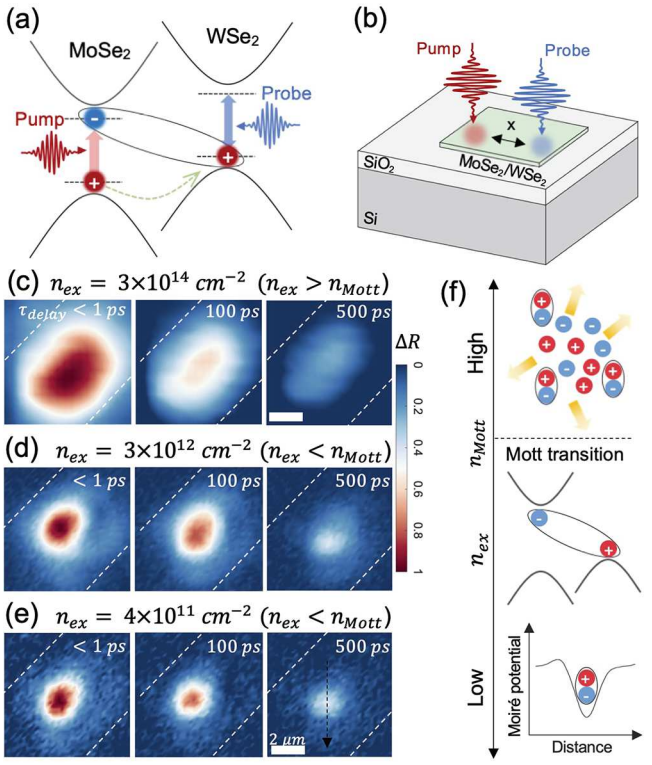

Figure 2. Spatial imaging of hot plasma transport and IX localization in the $MoSe_2/WSe_2$ TBL at T = 78 K. (a) Band diagram of the TBL and pump/probe pulses tuned to the $MoSe_2$ and WSe_2 intralayer A excitons, respectively. (b) Illustration of spatially resolved imaging of carrier or IX transport, where the probe beam is spatially scanned with respect to a fixed pump beam. Normalized transient differential reflection images at several delay times (τ_{delay} = <1, 100, and 500 ps) for (c) high ($n_{ex} = 3 \times 10^{14}$ cm^{-2}), (d) intermediate ($n_{ex} = 3 \times 10^{12}$ cm^{-2}), and (e) low ($n_{ex} = 4 \times 10^{11}$ cm^{-2}) excitation densities. White dashed lines indicate the boundary of the TBL region. Scale bar, 2 μm. (f) Illustration of the excitonic phase transition as a function of excitation density. At low density below n_{Mott}, IXs are localized by the moiré potential. Above the Mott density n_{Mott}, the electron–hole plasma expands rapidly.

expands almost instantaneously following the pump pulse. The spatial distribution appears elongated because the finite size of the TBL region restricts transport along one direction. No time evolution was observed within the images taken at delays of <1, 100, and 500 ps, besides a gradual signal decay due to carrier relaxation processes. In the low excitation-density images shown in Figure 2e, the nonlinear signal distribution remains localized within the excitation spot. Similarly, no temporal evolution of IX transport is observed with the population relaxation. We attribute this lack of temporal evolution to localization of IXs by the moiré potential consistent with earlier studies.[9,15,16,34−40] At the intermediate excitation density in Figure 2d, one can observe exciton diffusion mostly driven by dipolar repulsive interactions between interlayer excitons. In contrast, the extended spatial distribution of carriers at high excitation density ($n > n_{Mott}$) results from a rapid expansion of hot plasma that occurs beyond the limited temporal resolution of our experiment,[13,17,27] as illustrated in Figure 2f.

In Figure 3a, we directly compare line profiles of the spatial pump probe images. These line cuts are taken along a vertical direction (indicated by black arrow in Figure 2e) and fitted with a Gaussian function, $n(x, \tau) \propto \exp(-x^2/2\sigma_\tau^2)$, where σ_τ^2 corresponds to the variance. The spatial profile at low density is very close to the convoluted pump probe beam profile, and it remains so even for long delay times. This observation suggests that IXs diffusion at low density is impeded by the moiré potential, consistent with other studies.[9,13,16] By comparison, we can observe a stark difference between the high and low excitation density distributions near zero delay (σ_τ^2 of 5.56 ± 0.43 μm^2 vs 1.03 ± 0.03 μm^2), supporting the conclusion that the plasma expands rapidly within ~0.2 ps. To rule out possible artifacts due to nonlinear saturation effect, we examined the pump power-dependent nonlinear signal and its spatial profile at a fixed delay (details in SI). While Auger processes can lead to a fast relaxation dynamics and influence the spatial profile of the nonlinear signal,[41] it does not lead to observable changes in our case as shown via simulations included in SI.

Three line profiles at different delays at the highest excitation density show the same spatial extension with a decay in amplitude due to population relaxation (Figure 3b). Similar analyses at different excitation densities are performed and $\sigma^2_{\tau<1ps} - \sigma^2_{laser}$ near zero delay as a function of n_{ex} is

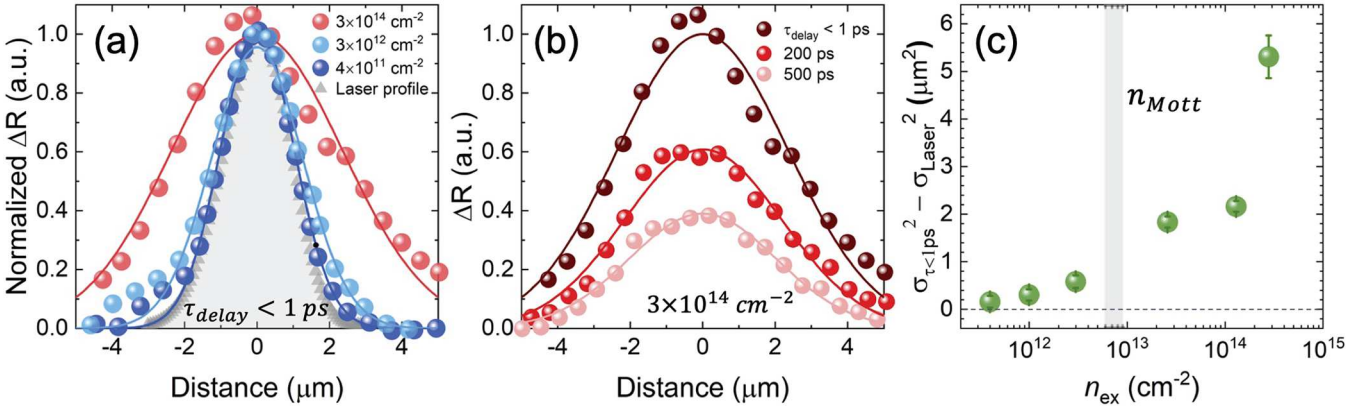

Figure 3. Detailed analysis of exciton and carrier transport at 78 K. (a) Comparison of line cuts of the nonlinear signal at short time delay of τ_{delay} < 1 ps for high (red), intermediate (light blue), and low (dark blue) excitation densities. Gray shaded Gaussian is the convoluted pump–probe profile in the low density measurement. (b) Delay-dependent spatial profiles of the nonlinear signal at high excitation density. (c) Excitation density dependent variance ($\sigma^2_{\tau<1ps} - \sigma^2_{laser}$). Vertical shaded stripe indicates the transition between bound IXs and ionized hot plasma beyond n_{Mott}.

https://doi.org/10.1021/acs.nanolett.3c00678
Nano Lett. 2023, 23, 4399−4405

displayed in Figure 3c. A gradual increase of expansion as excitation density increases is observed because of increased repulsive interactions between IXs. In the highest excitation density, the abrupt jump in σ_τ^2 results from the rapid hot plasma expansion driven by Fermi pressure, which will be explained in the following section. To ensure using two laser systems did not introduce ambiguity in drawing the main conclusion, We have carefully measured and deconvoluted pump and probe beam sizes in both systems and ruled out the difference between laser system as a possible cause for observing the strikingly rapid hot plasma expansion (details in SI).

To microscopically model the spatiotemporal dynamics of charge carriers, we introduce the Wigner function $\rho_{\lambda\mathbf{k}}(\mathbf{r}) = \sum_{\mathbf{q}} e^{i\mathbf{q}\cdot\mathbf{r}}\langle a^{\dagger}_{\lambda,\mathbf{k}-\frac{1}{2}\mathbf{q}} a_{\lambda,\mathbf{k}+\frac{1}{2}\mathbf{q}}\rangle$,[42−44] which is a quasi-probability function for carriers (electrons and holes denoted by λ = e, h) with the momentum $\mathbf{k}$ at the position $\mathbf{r}$. Here, the operator $a^{(\dagger)}_{\lambda\mathbf{k}}$ annihilates (creates) a charge carrier with the momentum $\mathbf{k}$. We consider a system of interacting charge carriers and phonons, where the carrier−carrier interaction is treated in a mean-field approximation. The equation of motion for the Wigner function in this system reads[45]

$$\dot{\rho}_{\lambda\mathbf{k}}(\mathbf{r},t) = -\mathbf{v}_{\lambda\mathbf{k}}\cdot\nabla_{\mathbf{r}}\rho_{\lambda\mathbf{k}}(\mathbf{r},t) + \sigma_\lambda\frac{1}{\hbar}\nabla_{\mathbf{r}}\Phi(\mathbf{r},t)\cdot\nabla_{\mathbf{k}}\rho_{\lambda\mathbf{k}}(\mathbf{r},t) + \dot{\rho}_{\lambda\mathbf{k}}(\mathbf{r},t)\Big|_{sc} \quad (1)$$

where σ_λ = +1 (−1) denotes the holes (electrons). The first term describes the free propagation of carriers with the velocity $\mathbf{v}_{\lambda\mathbf{k}} = \frac{1}{\hbar}\nabla_{\mathbf{k}}E_{\lambda\mathbf{k}} = \frac{\hbar\mathbf{k}}{m_\lambda}$. At sufficiently large densities, the Fermi level will rise above the band edge, and states with high kinetic energy will be occupied (Figure 4a). The higher velocity $\mathbf{v}_{\lambda\mathbf{k}}$ in

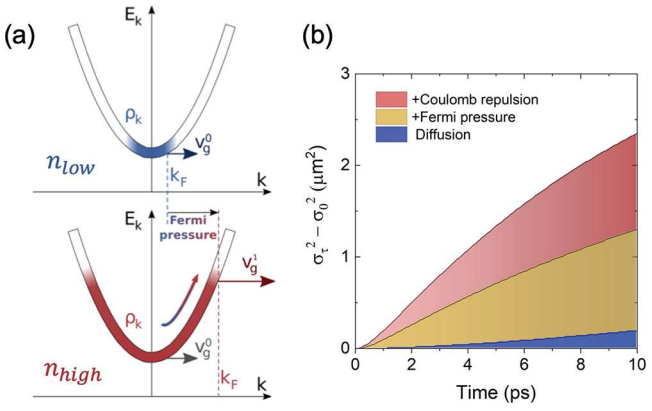

Figure 4. (a) Schematic illustration of the impact of Fermi pressure on carrier propagation. (b) Influence of hot plasma (blue), Fermi pressure (yellow), and Coulomb repulsion (red) on carrier diffusion for an initial excitation density of $n = 10^{14}$ cm^{-2}.

these states will result in an overall faster propagation. This effect is a direct consequence of Pauli's exclusion principle and is analogous to the phenomenon of Fermi pressure in neutron stars.[46−48]

The second term describes the acceleration of charge carriers due to their direct Coulomb interaction with other carriers. This effect is taken into account by the spatial gradient of the electrostatic potential $\Phi(\mathbf{r},t) = \int d^2\mathbf{r}' V(\mathbf{r}-\mathbf{r}')(n_h(\mathbf{r}',t) - n_e(\mathbf{r}',t))$. Here, $V(\mathbf{r})$ is the Coulomb potential and $n_\lambda(\mathbf{r},t) = A^{-1}\sum_{\mathbf{k}}\rho_{\lambda\mathbf{k}}(\mathbf{r},t)$ is the local carrier density with A being a normalization area of the crystal. In order to obtain an upper bound for the effect of Coulomb repulsion, we neglect the attraction between electrons and holes residing in different layers and only consider the repulsive interaction between particles of the same species. Many-particle screening may significantly reduce the Coulomb interaction at the high excitation density. We use the long wavelength static limit of the Lindhard formula[49] to account for this screening effect. Furthermore, $V(\mathbf{r})$ decays on a much shorter length-scale than $n_\lambda(\mathbf{r},t)$, and therefore, the electrostatic potential can be expressed as $\Phi(\mathbf{r},t) = \frac{e_0^2}{2\varepsilon\kappa(\mathbf{r},t)}n_h(\mathbf{r},t)$, where $\kappa(\mathbf{r},t) = \frac{e_0^2}{2\varepsilon}\frac{\partial n_h(\mathbf{r},t)}{\partial\mu}$ is the screening wavenumber and μ is the chemical potential. Exchange and correlation effects are not explicitly included in this formalism.

Finally, the last term in eq 1 describes local carrier−phonon scattering within the second-order Born-Markov approximation[50] and reads

$$\dot{\rho}_{\lambda\mathbf{k}}(\mathbf{r},t)|_{sc} = \sum_{\mathbf{k}'}\Gamma_{\mathbf{k}'\mathbf{k}}\rho_{\lambda\mathbf{k}'}(\mathbf{r},t)(1-\rho_{\lambda\mathbf{k}}(\mathbf{r},t)) - \Gamma_{\mathbf{k}\mathbf{k}'}\rho_{\lambda\mathbf{k}}(\mathbf{r},t)(1-\rho_{\lambda\mathbf{k}'}(\mathbf{r},t)) \quad (2)$$

Here, the Fermionic nature of electrons and holes manifests as Pauli blocking through the terms $1-\rho_{\lambda\mathbf{k}}(\mathbf{r},t)$. The matrix elements $\Gamma_{\mathbf{k}\mathbf{k}'}$ ensure energy and momentum conservation of the scattering process $\mathbf{k}\rightarrow\mathbf{k}'$ and contain the electron−phonon coupling strength, obtained in a deformation potential approximation with ab initio parameters from the previous study.[51]

The simulated carrier diffusion as a function of delay is summarized in Figure 4b. We assume at the initial time $t = 0$ that $\rho_{\lambda\mathbf{k}}(\mathbf{r}, t = 0)$ is well described by a Fermi−Dirac distribution at each position $\mathbf{r}$ and that $n_\lambda(\mathbf{r}, t = 0)$ follows a Gaussian profile. In addition to the effects described above, the carrier population is significantly heated under strong optical excitation. We model this effect by considering an initial thermal distribution with an effective temperature of up to 1000 K. While a hot plasma distribution should propagate faster than a colder one, we find that this effect is small at very high carrier densities in comparison to the impact of Fermi pressure and Coulomb repulsion, as shown in Figure 4b. The Fermi pressure effect (i.e., Pauli blocking) and Coulomb repulsion between carriers both contribute significantly to the rapid diffusion at high excitation density. When the charge density is increased, Pauli's exclusion principle forces electrons to occupy states with high momentum since low energy states are already full. The larger particle group velocities v_g consequently lead to a significantly faster propagation of electrons. Moreover, electron−phonon scattering channels are considerably quenched when the radius of the Fermi sphere k_F is increased, which additionally boosts the diffusivity.

The microscopic calculations identify Fermi pressure and Coulomb repulsion as the primary drivers of rapid carrier expansion at high excitation density. While falling short of full quantitative agreement, within only 8 ps the calculated change in variance reaches the experimental value at $\tau < 1$ ps ($\sigma_\tau^2 - \sigma_o^2 \approx 2\ \mu m^2$ for $n = 10^{14}$ cm^{-2}). Because the effective mass theory only applies to electrons in close vicinity to K valleys in our case, it may break down at the high instantaneous electron densities that immediately follow pump excitation. Unfortunately, a simulation of the spatiotemporal dynamics including

https://doi.org/10.1021/acs.nanolett.3c00678
Nano Lett. 2023, 23, 4399−4405

electrons across the whole Brillouin zone is not feasible. Other possible contributions might play a role at very high densities, e.g. screening of electron−phonon interactions or buildup of strong correlations that could explain the quantitative deviations from the experiment. Nevertheless, our microscopic calculations capture the main qualitative many-particle mechanisms behind the observed rapid carrier propagation at very high carrier densities.

In summary, we found that the exciton localization and hot plasma transport are highly tunable by the density in a $MoSe_2$/WSe_2 bilayer. This is a critical issue both for fundamental quantum science such as Mott physics and for optoelectronic applications in van der Waals heterostructures. Building on other recent high impact articles[13,27,52,53] using photoluminescence technique, our experiments use state-of-the-art pump/probe microscopy and provide higher spatial and temporal resolution (0.2 ps vs 10 ps or longer). Surprisingly, a hot plasma transport occurs over several microns in ∼0.2 ps. This rapid expansion is driven by Fermi pressure in addition to Coulomb repulsion at a density far exceeding the Mott transition. Hot plasma expansion is a topic of broad interests, relevant for distinct fields such as astrophysics and laser driven particle acceleration in addition to high-power optoelectronics.

■ ASSOCIATED CONTENT

Supporting Information

The Supporting Information is available free of charge at https://pubs.acs.org/doi/10.1021/acs.nanolett.3c00678.

Detailed descriptions of sample preparation, experimental methods (SHG, spatially resolved pump−probe spectroscopy, and PL) and complementary measurements (PDF)

■ AUTHOR INFORMATION

Corresponding Authors

Xiaoqin Li − *Department of Physics and Center for Complex Quantum Systems, The University of Texas at Austin, Austin, Texas 78712, United States;* orcid.org/0000-0002-2279-3078; Email: elaineli@physics.utexas.edu

Libai Huang − *Department of Chemistry, Purdue University, West Lafayette, Indiana 47907-2050, United States;* orcid.org/0000-0001-9975-3624; Email: libai-huang@purdue.edu

Authors

Junho Choi − *Department of Physics and Center for Complex Quantum Systems, The University of Texas at Austin, Austin, Texas 78712, United States;* Present Address: Advanced Instrumentation Institute, Korea Research Institute of Standards and Science, Daejeon 34113, Republic of Korea; orcid.org/0000-0002-8740-650X

Jacob Embley − *Department of Physics and Center for Complex Quantum Systems, The University of Texas at Austin, Austin, Texas 78712, United States*

Daria D. Blach − *Department of Chemistry, Purdue University, West Lafayette, Indiana 47907-2050, United States*

Raül Perea-Causín − *Department of Physics, Chalmers University of Technology, 41296 Gothenburg, Sweden*

Daniel Erkensten − *Department of Physics, Chalmers University of Technology, 41296 Gothenburg, Sweden;* orcid.org/0000-0002-9632-6376

Dong Seob Kim − *Department of Physics and Center for Complex Quantum Systems, The University of Texas at Austin, Austin, Texas 78712, United States*

Long Yuan − *Department of Chemistry, Purdue University, West Lafayette, Indiana 47907-2050, United States;* orcid.org/0000-0001-5591-9311

Woo Young Yoon − *Department of Electrical and Computer Engineering, The University of Texas at Austin, Austin, Texas 78712, United States*

Takashi Taniguchi − *International Center for Materials Nanoarchitectonics, National Institute for Materials Science, Tsukuba, Ibaraki 305-0044, Japan;* orcid.org/0000-0002-1467-3105

Kenji Watanabe − *Research Center for Functional Materials, National Institute for Materials Science, Tsukuba, Ibaraki 305-0044, Japan;* orcid.org/0000-0003-3701-8119

Keiji Ueno − *Department of Chemistry, Graduate School of Science and Engineering, Saitama University, Saitama 338-8570, Japan*

Emanuel Tutuc − *Department of Electrical and Computer Engineering, The University of Texas at Austin, Austin, Texas 78712, United States*

Samuel Brem − *Department of Physics, Philipps University of Marburg, 35037 Marburg, Germany;* orcid.org/0000-0001-8823-1302

Ermin Malic − *Department of Physics, Chalmers University of Technology, 41296 Gothenburg, Sweden; Department of Physics, Philipps University of Marburg, 35037 Marburg, Germany*

Complete contact information is available at: https://pubs.acs.org/10.1021/acs.nanolett.3c00678

Author Contributions

▼J.C., J.E., and D.D.B. contributed equally to this work.

Notes

The authors declare no competing financial interest.

■ ACKNOWLEDGMENTS

We gratefully acknowledge insightful discussions with Kyounghwan Kim for sample preparation. The spectroscopic studies performed by J.C. and X. Li were primarily supported by the Department of Energy, Basic Energy Science program via grant DE-SC0019398 and partially supported by NSF DMR-1808042 (J.E.) and NSF ECCS-2130552 (D.K.). The optical spectroscopy and microscopy work at Purdue (D.B., L.Y., and L.H.) are supported by the US Department of Energy, Office of Basic Energy Sciences, through award DE-SC0016356. Authors at UT-Austin acknowledge the use of facilities and instrumentation supported by the National Science Foundation through the Center for Dynamics and Control of Materials: an NSF MRSEC under Cooperative Agreement No. DMR-1720595. Material preparation was funded by the Welch Foundation via grant F-1662. K.W. and T.T. acknowledge support from JSPS KAKENHI (Grant Numbers 19H05790, 20H00354 and 21H05233). K. U. acknowledges support from the JSPS KAKENHI Grant No. 25107004. E.T. acknowledges support from the National Science Foundation Grant No. EECS-2122476. The Marburg group acknowledges support from Deutsche Forschungsgemeinschaft (DFG) via SFB 1083 (Project B9) and the European Unions Horizon 2020 research and innovation

https://doi.org/10.1021/acs.nanolett.3c00678
Nano Lett. 2023, 23, 4399−4405

program under grant agreement No 881603 (Graphene Flagship).

REFERENCES

(1) Rivera, P.; Schaibley, J. R.; Jones, A. M.; Ross, J. S.; Wu, S.; Aivazian, G.; Klement, P.; Seyler, K.; Clark, G.; Ghimire, N. J.; Yan, J.; Mandrus, D. G.; Yao, W.; Xu, X. Observation of long-lived interlayer excitons in monolayer mose2-wse2 heterostructures. *Nat. Commun.* **2015**, *6*, 6242.

(2) Choi, J.; Florian, M.; Steinhoff, A.; Erben, D.; Tran, K.; Kim, D. S.; Sun, L.; Quan, J.; Claassen, R.; Majumder, S.; Hollingsworth, J. A.; Taniguchi, T.; Watanabe, K.; Ueno, K.; Singh, A.; Moody, G.; Jahnke, F.; Li, X. Twist angle-dependent interlayer exciton lifetimes in van der waals heterostructures. *Phys. Rev. Lett.* **2021**, *126*, 047401.

(3) Kogar, A.; Rak, M. S.; Vig, S.; Husain, A. A.; Flicker, F.; Joe, Y. I.; Venema, L.; MacDougall, G. J.; Chiang, T. C.; Fradkin, E.; van Wezel, J.; Abbamonte, P. Signatures of exciton condensation in a transition metal dichalcogenide. *Science* **2017**, *358*, 1314.

(4) Wu, F.-C.; Xue, F.; MacDonald, A. H. Theory of two-dimensional spatially indirect equilibrium exciton condensates. *Phys. Rev. B* **2015**, *92*, 165121.

(5) Berman, O. L.; Kezerashvili, R. Y. High-temperature superfluidity of the two-component bose gas in a transition metal dichalcogenide bilayer. *Phys. Rev. B* **2016**, *93*, 245410.

(6) Debnath, B.; Barlas, Y.; Wickramaratne, D.; Neupane, M. R.; Lake, R. K. Exciton condensate in bilayer transition metal dichalcogenides: Strong coupling regime. *Phys. Rev. B* **2017**, *96*, 174504.

(7) Wang, Z.; Rhodes, D. A.; Watanabe, K.; Taniguchi, T.; Hone, J. C.; Shan, J.; Mak, K. F. Evidence of high-temperature exciton condensation in two-dimensional atomic double layers. *Nature* **2019**, *574*, 76.

(8) Jin, C.; Kim, J.; Utama, M. I. B.; Regan, E. C.; Kleemann, H.; Cai, H.; Shen, Y.; Shinner, M. J.; Sengupta, A.; Watanabe, K.; Taniguchi, T.; Tongay, S.; Zettl, A.; Wang, F. Imaging of pure spin-valley diffusion current in ws2-wse2 heterostructures. *Science* **2018**, *360*, 893.

(9) Yuan, L.; Zheng, B.; Kunstmann, J.; Brumme, T.; Kuc, A. B.; Ma, C.; Deng, S.; Blach, D.; Pan, A.; Huang, L. Twist-angle-dependent interlayer exciton diffusion in ws2−wse2 heterobilayers. *Nat. Mater.* **2020**, *19*, 617.

(10) Jauregui, L. A.; Joe, A. Y.; Pistunova, K.; Wild, D. S.; High, A. A.; Zhou, Y.; Scuri, G.; De Greve, K.; Sushko, A.; Yu, C.-H.; Taniguchi, T.; Watanabe, K.; Needleman, D. J.; Lukin, M. D.; Park, H.; Kim, P. Electrical control of interlayer exciton dynamics in atomically thin heterostructures. *Science* **2019**, *366*, 870.

(11) Rivera, P.; Seyler, K. L.; Yu, H. Y.; Schaibley, J. R.; Yan, J. Q.; Mandrus, D. G.; Yao, W.; Xu, X. D. Valley-polarized exciton dynamics in a 2d semiconductor heterostructure. *Science* **2016**, *351*, 688.

(12) Unuchek, D.; Ciarrocchi, A.; Avsar, A.; Sun, Z.; Watanabe, K.; Taniguchi, T.; Kis, A. Valley-polarized exciton currents in a van der waals heterostructure. *Nat. Nanotechnol* **2019**, *14*, 1104.

(13) Wang, J.; Shi, Q.; Shih, E.-M.; Zhou, L.; Wu, W.; Bai, Y.; Rhodes, D.; Barmak, K.; Hone, J.; Dean, C. R.; Zhu, X.-Y. Diffusivity reveals three distinct phases of interlayer excitons in $mose_2/wse_2$ heterobilayers. *Phys. Rev. Lett.* **2021**, *126*, 106804.

(14) Sun, Z.; Ciarrocchi, A.; Tagarelli, F.; Gonzalez Marin, J. F.; Watanabe, K.; Taniguchi, T.; Kis, A. Excitonic transport driven by repulsive dipolar interaction in a van der waals heterostructure. *Nat. Photonics* **2022**, *16*, 79.

(15) Brem, S.; Linderälv, C.; Erhart, P.; Malic, E. Tunable phases of moiré excitons in van der waals heterostructures. *Nano Lett.* **2020**, *20*, 8534.

(16) Choi, J.; Hsu, W.-T.; Lu, L.-S.; Sun, L.; Cheng, H.-Y.; Lee, M.-H.; Quan, J.; Tran, K.; Wang, C.-Y.; Staab, M.; Jones, K.; Taniguchi, T.; Watanabe, K.; Chu, M.-W.; Gwo, S.; Kim, S.; Shih, C.-K.; Li, X.; Chang, W.-H. Moiré potential impedes interlayer exciton diffusion in van der waals heterostructures. *Science Advances* **2020**, *6*, No. eaba8866.

(17) Fogler, M. M.; Butov, L. V.; Novoselov, K. S. High-temperature superfluidity with indirect excitons in van der waals heterostructures. *Nat. Commun.* **2014**, *5*, 4555.

(18) Ye, J. T.; Zhang, Y. J.; Akashi, R.; Bahramy, M. S.; Arita, R.; Iwasa, Y. Superconducting dome in a gate-tuned band insulator. *Science* **2012**, *338*, 1193.

(19) Lu, J. M.; Zheliuk, O.; Leermakers, I.; Yuan, N. F. Q.; Zeitler, U.; Law, K. T.; Ye, J. T. Evidence for two-dimensional ising superconductivity in gated mos2. *Science* **2015**, *350*, 1353.

(20) Costanzo, D.; Jo, S.; Berger, H.; Morpurgo, A. F. Gate-induced superconductivity in atomically thin mos2 crystals. *Nat. Nanotechnol.* **2016**, *11*, 339.

(21) Saito, Y.; Nakamura, Y.; Bahramy, M. S.; Kohama, Y.; Ye, J.; Kasahara, Y.; Nakagawa, Y.; Onga, M.; Tokunaga, M.; Nojima, T.; Yanase, Y.; Iwasa, Y. Superconductivity protected by spin−valley locking in ion-gated mos2. *Nat. Phys.* **2016**, *12*, 144.

(22) Castellanos-Gomez, A.; Buscema, M.; Molenaar, R.; Singh, V.; Janssen, L.; van der Zant, H. S. J.; Steele, G. A. Deterministic transfer of two-dimensional materials by all-dry viscoelastic stamping. *2D Materials* **2014**, *1*, 011002.

(23) Yu, H.; Liu, G.-B.; Yao, W. Brightened spin-triplet interlayer excitons and optical selection rules in van der waals heterobilayers. *2D Materials* **2018**, *5*, 035021.

(24) Zhang, L.; Gogna, R.; Burg, G. W.; Horng, J.; Paik, E.; Chou, Y.-H.; Kim, K.; Tutuc, E.; Deng, H. Highly valley-polarized singlet and triplet interlayer excitons in van der waals heterostructure. *Phys. Rev. B* **2019**, *100*, 041402.

(25) Ciarrocchi, A.; Unuchek, D.; Avsar, A.; Watanabe, K.; Taniguchi, T.; Kis, A. Polarization switching and electrical control of interlayer excitons in two-dimensional van der waals heterostructures. *Nat. Photonics* **2019**, *13*, 131.

(26) Stern, M.; Umansky, V.; Bar-Joseph, I. Exciton liquid in coupled quantum wells. *Science* **2014**, *343*, 55.

(27) Wang, J.; Ardelean, J.; Bai, Y.; Steinhoff, A.; Florian, M.; Jahnke, F.; Xu, X.; Kira, M.; Hone, J.; Zhu, X. Y. Optical generation of high carrier densities in 2d semiconductor heterobilayers. *Science Advances* **2019**, *5*, No. eaax0145.

(28) Chernikov, A.; Ruppert, C.; Hill, H. M.; Rigosi, A. F.; Heinz, T. F. Population inversion and giant bandgap renormalization in atomically thin ws2 layers. *Nat. Photonics* **2015**, *9*, 466.

(29) Steinhoff, A.; Florian, M.; Rösner, M.; Schönhoff, G.; Wehling, T. O.; Jahnke, F. Exciton fission in monolayer transition metal dichalcogenide semiconductors. *Nat. Commun.* **2017**, *8*, 1166.

(30) Bataller, A. W.; Younts, R. A.; Rustagi, A.; Yu, Y.; Ardekani, H.; Kemper, A.; Cao, L.; Gundogdu, K. Dense electron−hole plasma formation and ultralong charge lifetime in monolayer mos2 via material tuning. *Nano Lett.* **2019**, *19*, 1104.

(31) Siday, T.; Sandner, F.; Brem, S.; Zizlsperger, M.; Perea-Causin, R.; Schiegl, F.; Nerreter, S.; Plankl, M.; Merkl, P.; Mooshammer, F.; Huber, M. A.; Malic, E.; Huber, R. Ultrafast nanoscopy of high-density exciton phases in wse2. *Nano Lett.* **2022**, *22*, 2561.

(32) Moody, G.; Schaibley, J.; Xu, X. Exciton dynamics in monolayer transition metal dichalcogenides [invited]. *Journal of the Optical Society of America B* **2016**, *33*, C39.

(33) Jin, C.; Regan, E. C.; Wang, D.; Iqbal Bakti Utama, M.; Yang, C.-S.; Cain, J.; Qin, Y.; Shen, Y.; Zheng, Z.; Watanabe, K.; Taniguchi, T.; Tongay, S.; Zettl, A.; Wang, F. Identification of spin, valley and moiré quasi-angular momentum of interlayer excitons. *Nat. Phys.* **2019**, *15*, 1140.

(34) Jin, C.; Regan, E. C.; Yan, A.; Iqbal Bakti Utama, M.; Wang, D.; Zhao, S.; Qin, Y.; Yang, S.; Zheng, Z.; Shi, S.; Watanabe, K.; Taniguchi, T.; Tongay, S.; Zettl, A.; Wang, F. Observation of moire excitons in wse2/ws2 heterostructure superlattices. *Nature* **2019**, *567*, 76.

(35) Seyler, K. L.; Rivera, P.; Yu, H.; Wilson, N. P.; Ray, E. L.; Mandrus, D. G.; Yan, J.; Yao, W.; Xu, X. Signatures of moiré-trapped valley excitons in mose2/wse2 heterobilayers. *Nature* **2019**, *567*, 66.

(36) Tran, K.; Moody, G.; Wu, F.; Lu, X.; Choi, J.; Kim, K.; Rai, A.; Sanchez, D. A.; Quan, J.; Singh, A.; Embley, J.; Zepeda, A.; Campbell,

https://doi.org/10.1021/acs.nanolett.3c00678
Nano Lett. 2023, 23, 4399−4405

M.; Autry, T.; Taniguchi, T.; Watanabe, K.; Lu, N.; Banerjee, S. K.; Silverman, K. L.; Kim, S.; Tutuc, E.; Yang, L.; MacDonald, A. H.; Li, X. Evidence for moiré excitons in van der waals heterostructures. *Nature* **2019**, *567*, 71.
(37) Shabani, S.; Halbertal, D.; Wu, W.; Chen, M.; Liu, S.; Hone, J.; Yao, W.; Basov, D. N.; Zhu, X.; Pasupathy, A. N. Deep moiré potentials in twisted transition metal dichalcogenide bilayers. *Nat. Phys.* **2021**, *17*, 720.
(38) Zhang, C.; Chuu, C. P.; Ren, X.; Li, M. Y.; Li, L. J.; Jin, C.; Chou, M. Y.; Shih, C. K. Interlayer couplings, moire patterns, and 2d electronic superlattices in mos2/wse2 hetero-bilayers. *Science Advances* **2017**, *3*, No. e1601459.
(39) Alexeev, E. M.; Ruiz-Tijerina, D. A.; Danovich, M.; Hamer, M. J.; Terry, D. J.; Nayak, P. K.; Ahn, S.; Pak, S.; Lee, J.; Sohn, J. I.; Molas, M. R.; Koperski, M.; Watanabe, K.; Taniguchi, T.; Novoselov, K. S.; Gorbachev, R. V.; Shin, H. S.; Fal'ko, V. I.; Tartakovskii, A. I. Resonantly hybridized excitons in moiré superlattices in van der waals heterostructures. *Nature* **2019**, *567*, 81.
(40) Wu, F.; Lovorn, T.; MacDonald, A. H. Theory of optical absorption by interlayer excitons in transition metal dichalcogenide heterobilayers. *Phys. Rev. B* **2018**, *97*, 035306.
(41) Kulig, M.; Zipfel, J.; Nagler, P.; Blanter, S.; Schüller, C.; Korn, T.; Paradiso, N.; Glazov, M. M.; Chernikov, A. Exciton diffusion and halo effects in monolayer semiconductors. *Phys. Rev. Lett.* **2018**, *120*, 207401.
(42) Perea-Causin, R.; Brem, S.; Rosati, R.; Jago, R.; Kulig, M.; Ziegler, J. D.; Zipfel, J.; Chernikov, A.; Malic, E. Exciton propagation and halo formation in two-dimensional materials. *Nano Lett.* **2019**, *19*, 7317.
(43) Rosati, R.; Schmidt, R.; Brem, S.; Perea-Causin, R.; Niehues, I.; Kern, J.; Preuß, J. A.; Schneider, R.; Michaelis de Vasconcellos, S.; Bratschitsch, R.; et al. Dark exciton anti-funneling in atomically thin semiconductors. *Nat. Commun.* **2021**, *12*, 1.
(44) Brem, S.; Malic, E. Terahertz fingerprint of monolayer wigner crystals. *Nano Lett.* **2022**, *22*, 1311.
(45) Hess, O.; Kuhn, T. Maxwell-bloch equations for spatially inhomogeneous semiconductor lasers. i. theoretical formulation. *Phys. Rev. A* **1996**, *54*, 3347.
(46) van Driel, H. M. Kinetics of high-density plasmas generated in si by 1.06- and 0.53-μm picosecond laser pulses. *Phys. Rev. B* **1987**, *35*, 8166.
(47) Majumder, F. A.; Swoboda, H. E.; Kempf, K.; Klingshirn, C. Electron-hole plasma expansion in the direct-band-gap semiconductors cds and cdse. *Phys. Rev. B* **1985**, *32*, 2407.
(48) Ziebold, R.; Witte, T.; Hübner, M.; Ulbrich, R. G. Direct observation of fermi-pressure-driven electron-hole plasma expansion in gaas on a picosecond time scale. *Phys. Rev. B* **2000**, *61*, 16610.
(49) Haug, H.; Koch, S. W. *Quantum Theory of the Optical and Electronic Properties of Semiconductors*; World Scientific, 2009.
(50) Lindberg, M.; Koch, S. W. Effective bloch equations for semiconductors. *Phys. Rev. B* **1988**, *38*, 3342.
(51) Jin, Z.; Li, X.; Mullen, J. T.; Kim, K. W. Intrinsic transport properties of electrons and holes in monolayer transition-metal dichalcogenides. *Phys. Rev. B* **2014**, *90*, 045422.
(52) Sun, Z.; Ciarrocchi, A.; Tagarelli, F.; Gonzalez Marin, J. F.; Watanabe, K.; Taniguchi, T.; Kis, A. Excitonic transport driven by repulsive dipolar interaction in a van der waals heterostructure. *Nat. Photonics* **2022**, *16*, 79.
(53) Wagner, K.; Zipfel, J.; Rosati, R.; Wietek, E.; Ziegler, J. D.; Brem, S.; Perea-Causín, R.; Taniguchi, T.; Watanabe, K.; Glazov, M. M.; Malic, E.; Chernikov, A. Nonclassical exciton diffusion in monolayer wse_2. *Phys. Rev. Lett.* **2021**, *127*, 076801.

https://doi.org/10.1021/acs.nanolett.3c00678
Nano Lett. 2023, 23, 4399−4405